# OTS Physics-based Screening for Environment-friendly Selector Materials

D. Matsubayashi[2*], S. Clima[1], T. Ravsher[3], D. Garbin[1], R. Delhougne[1], G. S. Kar[1], and G. Pourtois[1,4]
[1]imec, Kapeldreef 75, B-3001 Leuven, Belgium; [2]KIOXIA Corporation assigned at imec; [3]KU Leuven, Celestijnenlaan 200D, B-3001 Leuven, Belgium; [4]PLASMANT, University of Antwerp, 2610 Antwerp, Belgium; *e-mail: Daisuke.Matsubayashi.ext@imec.be

*Abstract*— Restricted use of toxic elements is being explored extensively in the semiconductor industry for sustainable developments. In response to this trend, we performed systematic, and fully ab-initio screening for new ovonic threshold switching **(**OTS) ternary materials, excluding toxic elements such as As and Se. To narrow down the large amount of possible chemical compositions to the most promising candidates, we used OTS physics-based material parameters like material stability, electronic properties, or change in polarizability (OTS gauge). The OTS gauge concept is introduced as a condensed matter physics parameter to estimate the probability of a material to show an OTS behavior. As a result, we found 11 promising ternary compositions of As/Se-free OTS selector materials for RRAM applications.

## I. INTRODUCTION

High-capacity resistive random-access-memory (RRAM) array requires high performance 2-terminal selector devices in series with the RRAM cells to suppress sneak-path leakage currents (Fig. 1(a)). Ovonic threshold switching (OTS) is one of the promising physical mechanisms that can deliver the desired selector properties such that the leakage current through the device is orders of magnitude lower at half of threshold voltage, i.e., leading to high non-linearity (Fig. 1(b)) [1]. On the other hand, since mainstream OTS materials contain hazardous environmental chemicals such as As and Se [2-8], intensive studies to seek toxic-element-free materials have started to enable sustainable developments [9-12].

In this study, we report the first systematic screening for OTS materials using ab-initio simulations to identify new As/Se-free materials with a good OTS electrical behavior. We focused on ternary compounds and introduced eight screening filters to narrow down the promising candidates: undesirable and toxic element exclusion, amorphous phase stability at BEOL temperatures (high glass-transition temperature), OTS-compatible electronic configuration (~5 valence-electron rule), chemical stability (formation energy), selector application compatible electronic gap and traps, OTS behavior indicator (OTS gauge), and immunity to phase demixing (low spinodal temperature). The OTS gauge is introduced for the first time as a first-principle computable measure of the material to show an OTS behavior and has a strong correlation with experimental holding current. Through all these screening steps, we identified 17 materials that show promising OTS gauge, out of which only 11 OTS compositions are stable against demixing.

## II. PRE-SCREENING BEFORE AB-INITIO SIMULATION

To reduce the number of chemical compositions to be simulated, we applied three screening filters. The first screening filter is **element exclusion** to narrow down the combinations. We focused on 14 elements of B, C, N, Al, Si, P, S, Zn, Ga, Ge, In, Sn, Sb, and Te (Fig. 2), excluded As, Se and other toxic elements and excluded O in this study. All the possible ternary combinations of the **14 elements** with **10 % step** (atomic fraction) generated **13,104 compositions**. Fig. 3(a) shows frequency distribution of the mean number of valence electrons per atom ($N_{ve}$).

To identify thermally stable OTS materials to keep amorphous structures in the BEOL, we assumed the second screening filter of materials with glass-transition temperature $\boldsymbol{T_g}$ **higher than 600 K** within the requirements from typical BEOL temperature 400 °C (673.15 K). We roughly estimated $T_g$ of each composition using the Lankhorst model [13]. **6,596 compositions out of the 13,104 ones** were downselected by $T_g$ > 600 K (Fig. 3(b)).

The third screening filter is the **5 valence-electron rule** [14,15]. 5 valence electrons per atom need to populate one antibonding state, which makes bonding in some local regions unstable. This instability is needed to activate the OTS mechanism. We found a good correlation between $N_{ve}$ in the range of 5-5.3 and experimental holding voltage $V_{hold}$ for different compositions of SiGeAsSe, GeAsSe, and SiGeAsTe in the mushroom-type MIM devices (Fig. 3(c)), which consisted of 20nm-thick OTS materials deposited by PVD, TiN top and bottom (CD = 65nm) electrodes, and a ~10 kΩ series resistor. For the screening, we extracted **1,490 compositions with $N_{ve}$ = 5 ± 0.3 out of the 6,596 ones** (Fig. 3(b)).

## III. AB-INITIO METHODOLOGY

Our atomistic simulations are divided into two stages. The first stage is the generation of 10 amorphous models per composition by a decorate-and-relax algorithm. Each model is a 300-atom system with ~2x2x2 nm unit cell. To obtain high-quality atomistic models, we then optimized the structures using density functional theory (GTH pseudopotentials [16], DZVP localized basis sets, GGA-PBE [17]) using CP2K ab-initio software [18]. In the second stage, we computed the electronic gap using a hybrid functional method (HSE06/ ADMM [19]) and extracted mobility gap $E_\mu$, electron/hole trap levels $E_e$/$E_h$ and trap gap $\Delta E_t = E_e - E_h$ (Fig. 4 (a) (b)).

## IV. SCREENING AFTER AB-INITIO SIMULATION

To assess the chemical stability of an amorphous structure, we calculated the formation energy per atom $E_{form}$. Positive $E_{form}$ indicates a strong tendency to dealloying and atomic diffusion under thermal or electrical stress. Amorphous materials with positive $E_{form}$ are expected to have some reliability concerns leading to cyclic deterioration. Therefore, we imposed $\boldsymbol{E_{form} < 0}$ **eV/atom** for each composition as the fourth screening filter. $E_{form}$ of each amorphous model was estimated by the MEGNet model [20], which enables us to predict the formation energy by inputting the atomic coordinates of the model. **314 compositions out of the ab-**

**initio completed ones** were downselected using $E_{form} < 0$ eV/atom for median values of 10 models (Fig. 5).

Next, we considered large positive $\Delta E_t$ as a low leakage indicator, because zero energy trap gap incurs leakage mediated by gap states, preventing the OTS materials from being switched off. The fifth filter of $\Delta E_t > 0$ **eV** downselected **273 compositions out of the 314 ones** (see Fig. 5).

Fig. 6 summarizes the element breakdown of the screened compositions for each step. Note that the maximum percentage of each element is 33.3%, due to the ternary nature. After the fifth filter, almost all the compositions (31.9/33.3 = 93.1%) contain S, one of chalcogens. By contrast, the compositions containing Te are much lower (only 3.8/33.3 = 11.4%) and reduced by the second and fourth filters, suggesting that Te-containing compounds tend to be unstable.

To proceed further the downselection process, we defined **a window of $E_\mu$ and $\Delta E_t$** as the sixth screening filter. The window can change depending on target applications. For OTS materials with As/Se, we found a strong (weak) correlations between the computed $E_\mu$ ($\Delta E_t$) and experimental parameters such as threshold voltage $V_{th}$, first-fire voltage $V_{ff}$, and leakage current $I_{leak}$ [21]. This means that larger $E_\mu$ or $\Delta E_t$ induces higher $V_{th}$ and lower $I_{leak}$ (Fig. 7). Therefore, an optimal range of $E_\mu$ and $\Delta E_t$ should be defined based on the target applications. In this study, we defined **the target window of selector materials for RRAM as $E_\mu$ ~ 1.05-1.3 eV and $\Delta E_t$ ~ 0.4-0.6 eV**, corresponding to 2.5-3.8 V of $V_{th}$ range, to compromise read disturb and supply voltage. This window extracted **22 compositions out of the 273 ones** (Fig. 7). All of them contain S and none contain C, Al, and Zn.

To assess the probability of the 22 candidates to exhibit a good OTS behavior, we **introduced an OTS gauge,** based on Born effective charges ($Z^*$) which have been shown to be a good OTS indicator [22]. Fig. 8 shows the system charge dependence of $Z^*$ distribution for each element of SiGeAsSe-A (10 amorphous models with 300 atoms). The maximum and minimum values of $Z^*$ ($Z^*_{max/min}$) for each atom are separately plotted and the distributions broaden with increasing the system charges ($q = 0 \rightarrow \pm 2e \rightarrow \pm 4e$) in the positive/negative direction for $Z^*_{max/min}$, respectively. This means that the injection of electrons and holes to the system, followed by their trapping in the defective levels, induces additional $Z^*$. Such an increase is considered as a sign of OTS switching. To quantify this tendency, we formulated the OTS gauge as shown in Fig. 9.

Fig. 10 shows comparison of OTS gauges for existing OTS materials (SiGeAsSe, GeAsSe, GeSe, SiGeAsTe, SiTe), non-OTS materials as reference (c-AlN, c-$Al_2O_3$, c-$HfO_2$, c-$SiO_2$), and As/Se-free OTS candidates. Existing OTS materials have relatively large values (18-62) compared to the non-OTS ones (1-2). In addition, we found that strong positive correlation of the OTS gauge with experimental holding current $I_{hold}$ (Fig. 11). Therefore, a material with a large OTS gauge should have high $I_{hold}$ and high non-linearity, namely a good OTS behavior.

Since the OTS gauge defined above was verified as a quantitative OTS indicator, we applied it as an additional screening filter on the remaining 22 OTS candidates. All have a similar range of OTS gauges (7-58) as obtained for the existing OTS materials, but 5 compositions have values < 18. Therefore, the seventh filter of **OTS gauge > 18 extracted 17 compositions out of the 22 ones**.

For the final screening in this study, we discussed the phase stability of the OTS candidates in terms of spinodal temperature $T_{spinodal}$ [23]. For example, $S_{0.5}Ge_{0.1}Sn_{0.4}$, one of the candidates, is surrounded by SnS, $SnGeS_3$, and Ge on the crystalline phase diagram of the S-Ge-Sn system (Fig. 12 (a)) [24,25]. This means that $S_{0.5}Ge_{0.1}Sn_{0.4}$ has a risk to demix into these three systems. To confirm the phase stability of this composition, the estimation of $T_{spinodal}$ is needed (Fig. 12 (b)). For a given-temperature $T > T_{spinodal}$, the mixing entropy stabilizes the alloy structure. Meanwhile, for $T < T_{spinodal}$, the mixing entropy does not help stabilizing the alloy, which then has a high risk of demixing. Therefore, $T_{spinodal}$ is desired to be as low as possible to promote alloying stability.

To estimate $T_{spinodal}$, we need to know the second derivative of the $E_{form}$ with respect to composition change on the phase diagram. Since the data points on the phase diagram were too few to calculate the curvature, we created a prediction model of amorphous $E_{form}$ for any arbitrary compositions, using machine learning (ML) technique (support vector machine [26]). The ML dataset contained 8,260 $E_{form}$ data of amorphous compounds with ternary/binary compositions and single-element crystals. 90% of the dataset was used for training and 10% for testing. Fig. 13 (a) and (b) show predicted $E_{form}$ on the crystalline phase diagram of the S-Ge-Sn system and along the compositions of $S_{0.5}Ge_xSn_{0.5-x}$, respectively. The prediction model reproduced the original data (Fig. 13 (b) (c)).

We evaluated $T_{spinodal}$ of the 22 OTS candidates, based on the prediction model (Fig. 14). 12 compositions including $S_{0.5}Ge_{0.1}Sn_{0.4}$ had $T_{spinodal}$ of 0 K so that they were expected to be stable at any temperature. Since a typical deposition temperature of OTS materials is room temperature to 100 °C, we imposed $T_{spinodal} < 0$ **°C (273.15 K)** as the eighth filter, which downselected **11 phase-stable compositions out of the 17 ones** extracted previously. Table. I summarizes the parameters of the 11 promising OTS compositions of selector materials for RRAM, satisfying all the eight filters at the same time. In terms of OTS gauge, $P_{0.2}S_{0.4}Ge_{0.4}$, $Si_{0.3}S_{0.5}Sn_{0.2}$ and $Si_{0.3}S_{0.5}Ge_{0.2}$ are expected to be the most promising materials.

## V. CONCLUSIONS

We established the first systematic method of the ab-initio screening for new OTS materials, by introducing the eight screening filters: element exclusions, $T_g$ > 600 K, 5 valence-electron rule, $E_{form} < 0$ eV/atom, $\Delta E_t > 0$ eV, $E_\mu$ - $\Delta E_t$ target window, OTS gauge > 18, and $T_{spinodal} < 0$ °C. This OTS physics-based method identified 11 promising ternary compositions of As/Se-free OTS selector materials for RRAM starting from 13,104 candidates. The same procedure is applicable to other target applications such as stand-alone self-rectified memory devices [27].


## ACKNOWLEDGMENT

This work was carried out in the framework of the imec Core CMOS – Active Memory Program.

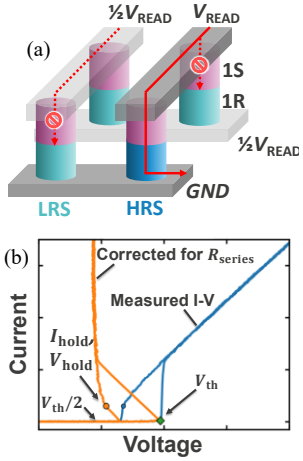


Fig.1. (a) Schematic role of the selector devices in series with resistive memory element (1S1R), which cut the parasitic leakage on half-biased low-resistance-state (LRS) memory cells, while allowing the correct reading of a high-resistance-state (HRS) memory cell. (b) Typical I-V characteristics of an OTS selector device with series resistance $R_{series}$.

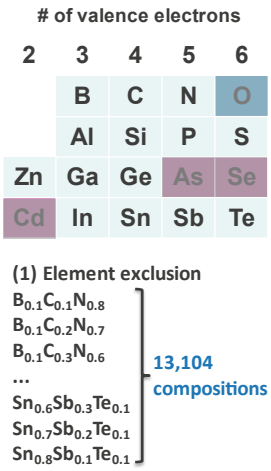


Fig. 2. The first screening filter of element exclusion for new OTS materials. This selected 14 elements of B, C, N, Al, Si, P, S, Zn, Ga, Ge, In, Sn, Sb and Te, excluded As, Se and other toxic elements, and excluded O in this study. All the possible ternary combinations with 10% atomic fraction step generated 13,104 compositions.

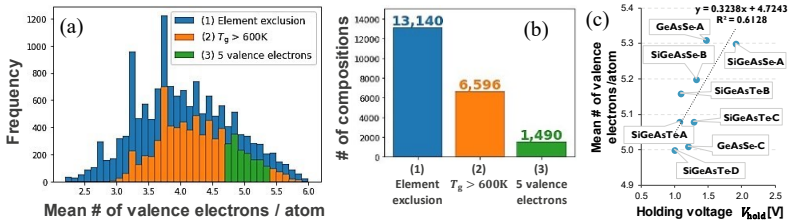


Fig. 3. (a) Frequency distribution of the screened compositions for the mean number of valence electrons per atom $N_{ve}$ and (b) the number of compositions after the 3 screening filters of (1) element exclusion, (2) glass-transition temperature $T_g$ higher than 600 K, and (3) 5 valence-electron rule ($N_{ve} = 5 \pm 0.3$). (c) Good correlation between $N_{ve}$ and experimental holding voltage $V_{hold}$ for different OTS materials with As/Se.

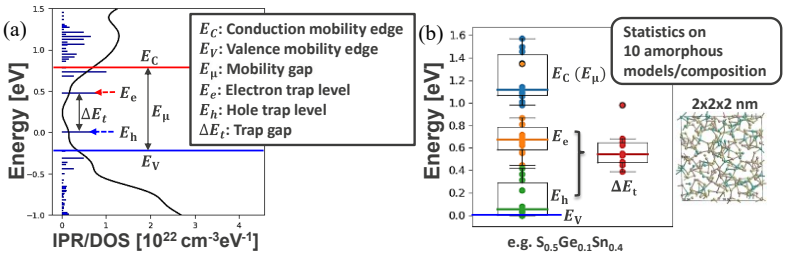


Fig. 4. (a) Ab-initio calculation results of the inverse participation ratio (IPR, horizontal bars showing state localization degree) and the density of states (DOS), used to extract the conduction/valence edges, electron/hole trap levels, and mobility gap. (b) Extracted electron/hole trap levels and mobility gaps for 10 amorphous models (300 atoms ~2x2x2 nm) per chemical composition.

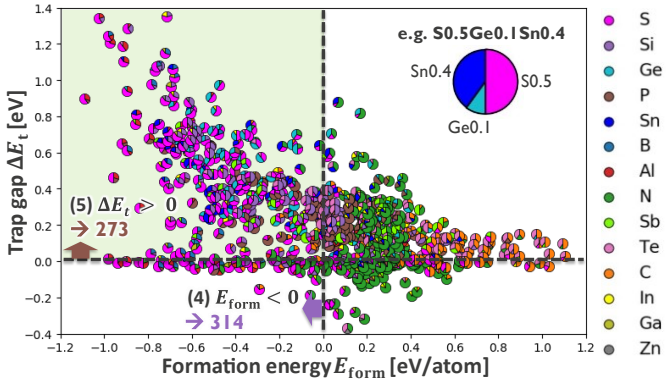


Fig. 5. Formation energy $E_{form}$ and trap gap $\Delta E_t$ (median values of 10 amorphous models) of ab-initio completed compositions, screened by the two filters of (4) amorphous structure stability $E_{form} < 0$ eV/atom and (5) less leakage $\Delta E_t > 0$ eV. Atomic fractions of each composition are expressed by pie-chart.

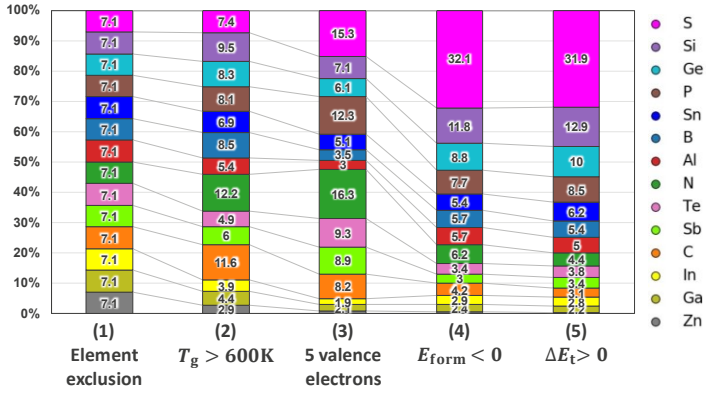


Fig. 6. Element breakdown of screened compositions for each screening step. Possible maximum percentage of each element is 33.3% due to the ternary nature. After the fifth filter, almost all alloys contain S.

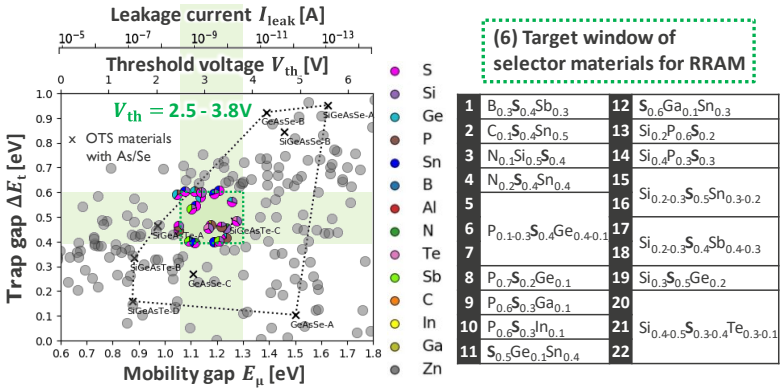


(6) Target window of selector materials for RRAM

| | | | |
|---|---|---|---|
| 1 | $B_{0.3}S_{0.4}Sb_{0.3}$ | 12 | $S_{0.6}Ga_{0.1}Sn_{0.3}$ |
| 2 | $C_{0.1}S_{0.4}Sn_{0.5}$ | 13 | $Si_{0.2}P_{0.6}S_{0.2}$ |
| 3 | $N_{0.1}Si_{0.5}S_{0.4}$ | 14 | $Si_{0.4}P_{0.3}S_{0.3}$ |
| 4 | $N_{0.2}S_{0.4}Sn_{0.4}$ | 15 | $Si_{0.2\text{-}0.3}S_{0.5}Sn_{0.3\text{-}0.2}$ |
| 5 | $P_{0.1\text{-}0.3}S_{0.4}Ge_{0.4\text{-}0.1}$ | 16 | |
| 6 | | 17 | $Si_{0.2\text{-}0.3}S_{0.4}Sb_{0.4\text{-}0.3}$ |
| 7 | | 18 | |
| 8 | $P_{0.7}S_{0.2}Ge_{0.1}$ | 19 | $Si_{0.3}S_{0.5}Ge_{0.2}$ |
| 9 | $P_{0.6}S_{0.3}Ga_{0.1}$ | 20 | $Si_{0.4\text{-}0.5}S_{0.3\text{-}0.4}Te_{0.3\text{-}0.1}$ |
| 10 | $P_{0.6}S_{0.3}In_{0.1}$ | 21 | |
| 11 | $S_{0.5}Ge_{0.1}Sn_{0.4}$ | 22 | |

Fig. 7. Mobility gap $E_\mu$ and trap gap $\Delta E_t$ (median values of 10 amorphous models) of the screened compositions up to the fifth filter. $V_{th}$ and $I_{leak}$ of the upper horizontal axes were coverted from $E_\mu$ using the correlation in OTS materials with As/Se. A target window of selector materials for RRAM is defined as $E_\mu$ ~ 1.05-1.3 eV and $\Delta E_t$ ~ 0.4-0.6 eV, which corresponds to 2.5-3.8 V of $V_{th}$ range. This target window filter (6) downselected 22 compositions out of the 273 ones.

## REFERENCES


[1] S. R. Ovshinsky, PRL 21, 1450 (1968). [2] H. Y. Cheng et al., IEDM 2017. [3] S. Clima et al., IEDM 2017. [4] B. Govoreanu et al., VLSI 2017. [5] H. Y. Cheng et al., IEDM 2018. [6] D. Garbin et al., IEDM 2019. [7] S. Kabuyanagi et al., VLSI 2020. [8] H. Y. Cheng et al., IEDM 2021. [9] S. Jia et al., Nat. Commun. 11, 4636 (2020). [10] C. H. Wu et al., VLSI 2021. [11] E. Ambrosi et al., IEDM 2021. [12] S. Hatayama et al., APL Mater. 10, 011106 (2022). [13] M. H. R. Lankhorst, J. Non-Cryst. Solids 297, 210 (2002). [14] M. B. Luo et al., Adv. Mater. 16, 439 (2004). [15] H. L. Li et al., Sci. Rep. 9, 1867 (2019). [16] S. Goedecker et al., PRB 54, 1703 (1996). [17] J. P. Perdew et al., PRL 77, 3865 (1996). [18] J. Hutter et al., Wiley Interdiscip. Rev. Comput. Mol. Sci. 4, 15 (2014). [19] M. Guidon et al., J. Chem. Theory Comput. 6, 2348 (2010). [20] C. Chen et al., Chem. Mater. 31, 3564 (2019). [21] S. Clima et al., manuscript in preparation. [22] P. Noé et al., Sci. Adv. 6, eaay2830 (2020). [23] S. Zhang et al., JAP 114, 133510 (2013). [24] S. P. Ong et al., Chem. Mater. 20, 1798 (2008). [25] A. Jain et al., PRB 84, 045115 (2011). [26] C. Cortes et al., Mach. Learn. 20, 273 (1995). [27] T. Ravsher et al., VLSI 2022.

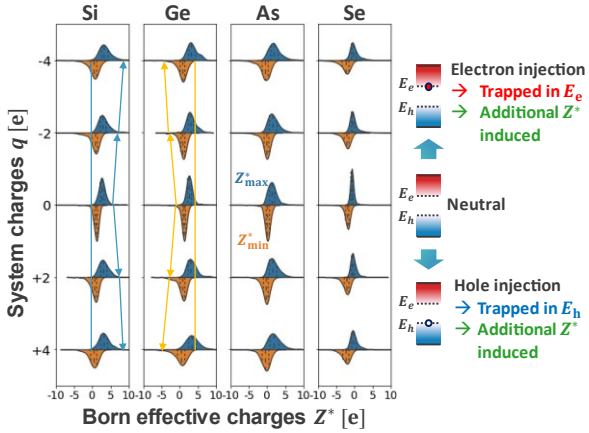


Fig. 8. System charge dependence of Born effective charge $Z^*$ distribution for each element of SiGeAsSe-A. 10 amorphous models with 300 atoms were considered. The distributions broaden with increasing system charges, in the positive/negative direction for $Z^*_{max/min}$, respectively. Injected electrons/holes are trapped in the electron/hole trap levels, respectively, and induce additional $Z^*$.

- **Born effective charge ($Z^*$) for each atom $i$ in a system $k$**

$$Z^*_{k,i,ab} = \frac{\partial F_{k,i,a}}{\partial E_b} \quad (a,b = x,y,z)$$

- **Max/min value of the diagonal terms**

$$Z^*_{\max/\min,k,i} = \max/\min(\mathrm{diag}\, Z^*_{k,i,ab})$$

- **Total max/min $Z^*$ per system (the number of systems, $n$)**

$$Z^*_{\max/\min,\mathrm{tot}} = \sum_{k,i} Z^*_{\max/\min,k,i}\,/n$$

- **Induced total max/min $Z^*$ by system charges $q$**

$$\Delta Z^*_{\max/\min,\mathrm{tot}}(q) = Z^*_{\max/\min,\mathrm{tot}}(q) - Z^*_{\max/\min,\mathrm{tot}}(0)$$

- **Induced total max/min $Z^*$ per unit system charge $\pm e$**

$$S^{\pm}_{\max/\min} = \frac{d\Delta Z^*_{\max/\min,\mathrm{tot}}(q)}{dq}\Big|_{q=\pm e}$$

- **Mean value of $|S^{\pm}_{\max/\min}|$**

$$\mathrm{OTS\ gauge} = \sum_{\pm,\,\max/\min} |S^{\pm}_{\max/\min}|/4$$

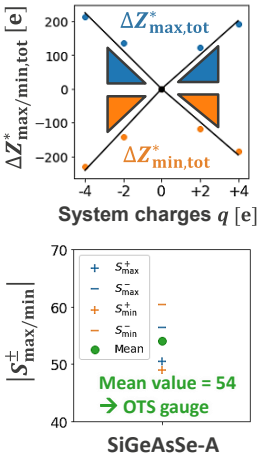


Fig. 9. Definition of OTS gauge and the value for SiGeAsSe-A as an example. The values of $S^{\pm}_{max/min}$ were estimated to be the four slopes of the approximated lines for $\Delta Z^*_{max/min,tot}(q)$ at $q$ = 0/±2e/±4e. The OTS gauge was defined as the mean value of $|S^{\pm}_{max/min}|$.

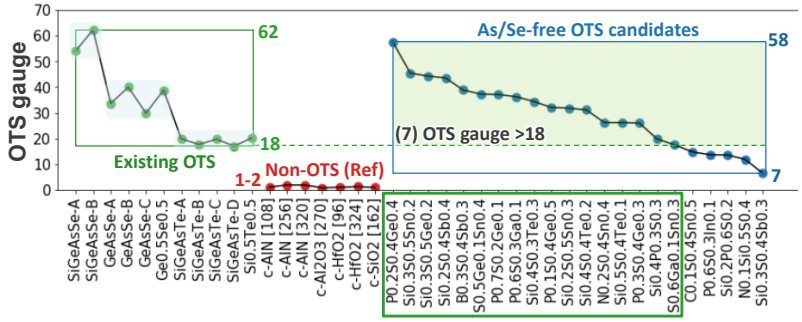


Fig. 10. Comparison of OTS gauges for existing OTS materials (SiGeAsSe, GeAsSe, GeSe, SiGeAsTe, SiTe), non-OTS materials (c-AlN, c-$Al_2O_3$, c-$HfO_2$, c-$SiO_2$), and As/Se-free OTS candidates. The number in square brackets for the non-OTS materials depicts the number of atoms in a unit cell. (7) OTS gauge > 18 filtered down to 17 compositions out of the 22 candidates.

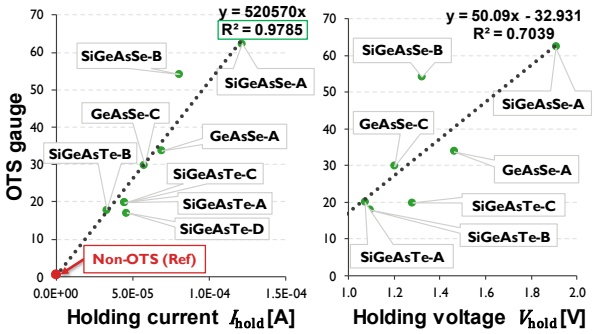


Fig. 11. OTS gauge and experimental holding current/voltage $I_{hold}/V_{hold}$ of the OTS materials with As/Se. The OTS gauge has a strong positive correlation with $I_{hold}$.

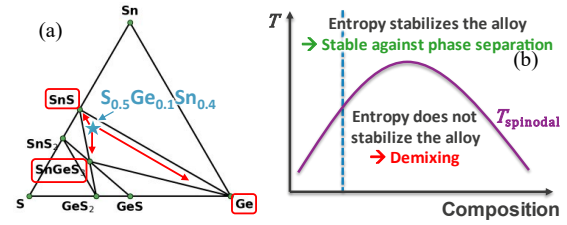


Fig. 12. (a) Phase stability of $S_{0.5}Ge_{0.1}Sn_{0.4}$ on the crystalline phase diagram of S-Ge-Sn system. $S_{0.5}Ge_{0.1}Sn_{0.4}$ has a risk to demix into SnS, $SnGeS_3$, and Ge. (b) Schematic of the spinodal temperature $T_{spinodal}$, which is desired to be as low as possible for phase stability.

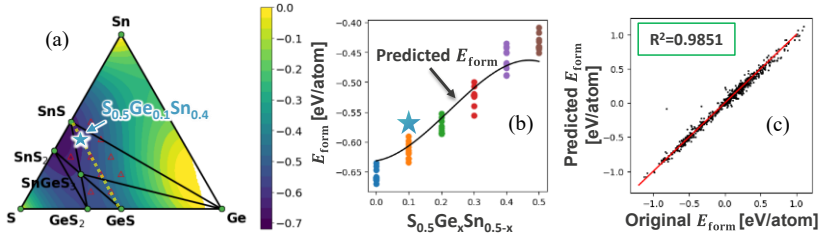


Fig. 13. (a) Predicted formation energy $E_{form}$ on the crystalline phase diagram of S-Ge-Sn system. (b) Comparison of $E_{form}$ between 10 amorphous data and prediction data based on machine learning, along the compositions of $S_{0.5}Ge_xSn_{0.5-x}$. (c) Overall accuracy of the prediction model for $E_{form}$.

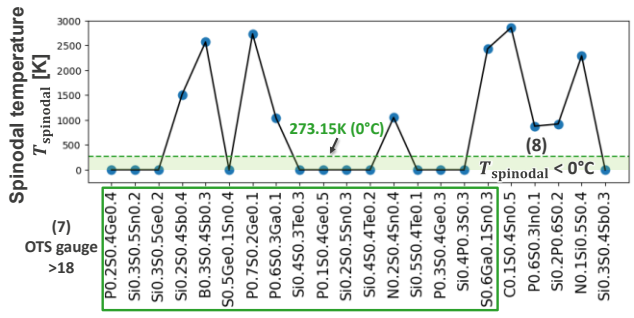


Fig. 14. Estimated spinodal temperature $T_{spinodal}$ of the 22 OTS candidates. 11 compositions were downselected by the filter (8) $T_{spinodal}$ < 0 °C, out of the 17 compositions with OTS gauge > 18.

Table. I. Summary of 11 promising OTS compositions of selector materials for RRAM

| | Composition | OTS gauge | $T_{spinodal}$ [K] | $E_g$ [eV] | $\Delta E_t$ [eV] | $E_{form}$ [eV/atom] | $N_{ve}$ | $T_g$ [K] |
|---|---|---|---|---|---|---|---|---|
| 1 | $P_{0.2}S_{0.4}Ge_{0.4}$ | 58 | 0 | 1.05 | 0.59 | -0.41 | 5.0 | 712 |
| 2 | $Si_{0.3}S_{0.5}Sn_{0.2}$ | 45 | 0 | 1.08 | 0.61 | -0.68 | 5.0 | 823 |
| 3 | $Si_{0.3}S_{0.5}Ge_{0.2}$ | 44 | 0 | 1.26 | 0.56 | -0.57 | 5.0 | 871 |
| 4 | $S_{0.5}Ge_{0.1}Sn_{0.4}$ | 37 | 0 | 1.12 | 0.54 | -0.62 | 5.0 | 662 |
| 5 | $Si_{0.4}S_{0.3}Te_{0.3}$ | 34 | 0 | 1.17 | 0.45 | -0.37 | 5.2 | 728 |
| 6 | $P_{0.1}S_{0.4}Ge_{0.5}$ | 32 | 0 | 1.14 | 0.58 | -0.38 | 4.9 | 734 |
| 7 | $Si_{0.2}S_{0.5}Sn_{0.3}$ | 32 | 0 | 1.19 | 0.59 | -0.67 | 5.0 | 768 |
| 8 | $Si_{0.4}S_{0.4}Te_{0.2}$ | 31 | 0 | 1.27 | 0.48 | -0.53 | 5.2 | 784 |
| 9 | $Si_{0.5}S_{0.4}Te_{0.1}$ | 26 | 0 | 1.14 | 0.60 | -0.52 | 5.0 | 868 |
| 10 | $P_{0.3}S_{0.4}Ge_{0.3}$ | 26 | 0 | 1.11 | 0.60 | -0.40 | 5.1 | 698 |
| 11 | $Si_{0.4}P_{0.3}S_{0.3}$ | 20 | 0 | 1.05 | 0.46 | -0.34 | 4.9 | 913 |